Bulletin of the Seismological Society of America, Vol. 94, No. 1, pp. 131–146, February 2004

# Observed and Simulated Ground Motions in the San Bernardino Basin Region for the Hector Mine, California, Earthquake

by Robert W. Graves and David J. Wald

**Abstract** During the $M_w$ 7.1 Hector Mine earthquake, peak ground velocities recorded at sites in the central San Bernardino basin region were up to 2 times larger and had significantly longer durations of strong shaking than sites just outside the basin. To better understand the effects of 3D structure on the long-period ground-motion response in this region, we have performed finite-difference simulations for this earthquake. The simulations are numerically accurate for periods of 2 sec and longer and incorporate the detailed spatial and temporal heterogeneity of source rupture, as well as complex 3D basin structure. Here, we analyze three models of the San Bernardino basin: model A (with structural constraints from gravity and seismic reflection data), model F (water well and seismic refraction data), and the Southern California Earthquake Center version 3 model (hydrologic and seismic refraction data). Models A and F are characterized by a gradual increase in sediment thickness toward the south with an abrupt step-up in the basement surface across the San Jacinto fault. The basin structure in the SCEC version 3 model has a nearly uniform sediment thickness of 1 km with little basement topography along the San Jacinto fault. In models A and F, we impose a layered velocity structure within the sediments based on the seismic refraction data and an assumed depth-dependent $V_p/V_s$ ratio. Sediment velocities within the SCEC version 3 model are given by a smoothly varying rule-based function that is calibrated to the seismic refraction measurements. Due to computational limitations, the minimum shear-wave velocity is fixed at 600 m/sec in all of the models. Ground-motion simulations for both models A and F provide a reasonably good match to the amplitude and waveform characteristics of the recorded motions. In these models, surface waves are generated as energy enters the basin through the gradually sloping northern margin. Due to the basement step along the San Jacinto fault, the surface wave energy is confined to the region north of this structure, consistent with the observations. The SCEC version 3 model, lacking the basin geometry complexity present in the other two models, fails to provide a satisfactory match to the characteristics of the observed motions. Our study demonstrates the importance of using detailed and accurate basin geometry for predicting ground motions and also highlights the utility of integrating geological, geophysical, and seismological observations in the development and validation of 3D velocity models.

## Introduction

The 1999 Hector Mine earthquake ($M_w$ 7.1) is the largest event to be recorded on the recently installed TriNet strong motion system in southern California. The event ruptured over at least three main fault segments in the Mojave desert about 100 km east-northeast of the San Bernardino Valley (e.g., Hauksson *et al.*, 2002) (Fig. 1). This valley contains major transportation routes and large-scale industrial and business complexes, as well as a large population base. Although little damage to the built environment occurred during the Hector Mine event, the density of strong motion recording sites in the San Bernardino region provides an unprecedented opportunity to examine source, wave propagation, and basin response effects during a major earthquake in southern California. Geologically, the San Bernardino Valley is underlain by a wedge-shaped sedimentary basin that is formed by the intersection of the San Andreas and San Jacinto faults (Fig. 2). The segments of these faults adjacent to the valley are quite active and have been given the

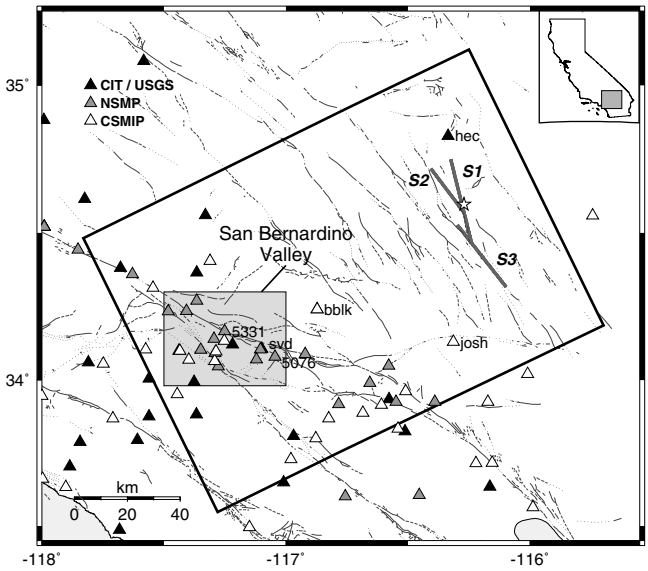


Figure 1. Map of the southern California region including the Hector Mine earthquake rupture and the San Bernardino Valley. The three segments of the Ji *et al.* (2002) rupture model are labeled S1, S2, and S3, with the epicenter indicated by the star. Strong motion instruments that recorded the mainshock are shown by triangles. The large rectangle depicts the area covered by the FD model (116 km × 162 km). A more detailed view of the San Bernardino Valley region, which is indicated by the gray-shaded rectangle, is shown in Figure 2.

highest probabilities of rupture for type-A faults in southern California (WGCEP, 1995). Furthermore, the presence of complex stratigraphy and laterally varying geology in this region adds to the complexity of the situation. The combination of a large population density, extensive built environment, geologic complexity, and high probability of rupture on these faults stresses the importance for understanding the ground-shaking hazard within the valley region.

The first detailed studies of ground-motion response in the San Bernardino region were conducted by Frankel (1993, 1994). In Frankel (1993), a preliminary model of the 3D basin structure was developed using water well (Dutcher and Garrett, 1963) and seismic refraction data (Hadley and Combs, 1974). This model was relatively simple, consisting of a single (constant-velocity) sedimentary unit embedded in a homogeneous half-space. Frankel (1993) used this model to simulate long-period ground motions for $M_w$ 6.5 scenario earthquakes on the San Andreas fault immediately adjacent to the basin. The simulated motions showed significant basin amplification and rupture directivity effects in the period range of 1–4 sec. Following this original study, Frankel (1994) analyzed aftershocks of the 1992 Landers and Big Bear earthquakes that were recorded on temporary arrays situated in the San Bernardino region. This study found that sites within the basin had significant amplification and much longer durations of shaking relative to sites located outside of the basin. In addition, array analysis of these weak motion data showed that the late-arriving energy is dominated by surface waves propagating in various directions across the basin. Using his relatively simple 3D basin model, Frankel (1994) was able to reproduce the general characteristics of the basin response for these small events. Unfortunately, the Landers and Big Bear mainshocks were not well recorded at sites in the basin, precluding any direct comparison of the simulations with data from these larger events.

Several recent studies have been conducted to help delineate the detailed subsurface structure of the basin geometry in the San Bernardino region. These include Anderson *et al.* (2000a,b) and Langenheim *et al.* (2002), who used potential field data to develop a 3D model of the basement topography underlying the basin, and Stephenson *et al.* (2002), who analyzed seismic reflection data gathered along a northeast–southwest profile across the basin (see Fig. 2). The basin structure inferred from these studies is characterized by a basement surface that dips gradually toward the southwest and reaches a maximum depth of about 1.6–1.8 km just north of the San Jacinto fault. In these models, the basin is significantly shallower to the south and west of the San Jacinto fault. A different representation of the basin structure is provided by the Southern California Earthquake Center (SCEC) version 3 seismic velocity model (Kohler *et al.*, 2003). This model is characterized by a sharp step in the basement surface along the San Andreas fault and a nearly uniform sediment depth of 1 km throughout the basin. Furthermore, the SCEC model shows little variation in the basement topography across the San Jacinto fault.

Our objective in this study is to analyze the sensitivity of the ground-motion response to the differences in the proposed basin models and to compare the simulated and observed motions to delineate which model features produce characteristics similar to those seen in the Hector Mine data. Ultimately, our goal is to use constraints provided by these studies to develop a more comprehensive and robust model of the basin structure and ground-motion response in the San Bernardino region.

## Observed Ground Motions

The Hector Mine earthquake was recorded by well over 100 strong motion instruments throughout southern California. Due to the remote location of the earthquake, the density of recording sites was relatively sparse in the near-fault region; however, the number of observation sites increases substantially in the more populated areas (Fig. 1). The San Bernardino Valley, at a distance of about 90–100 km, represents the closest approach of large-scale urban development to the fault rupture. Records from about 20 strong motion sites were obtained in the immediate vicinity of the San Bernardino region during the Hector Mine mainshock (Fig. 2). These sites are located within the basin itself and along its margins.

To analyze these ground-motion records, we first plot

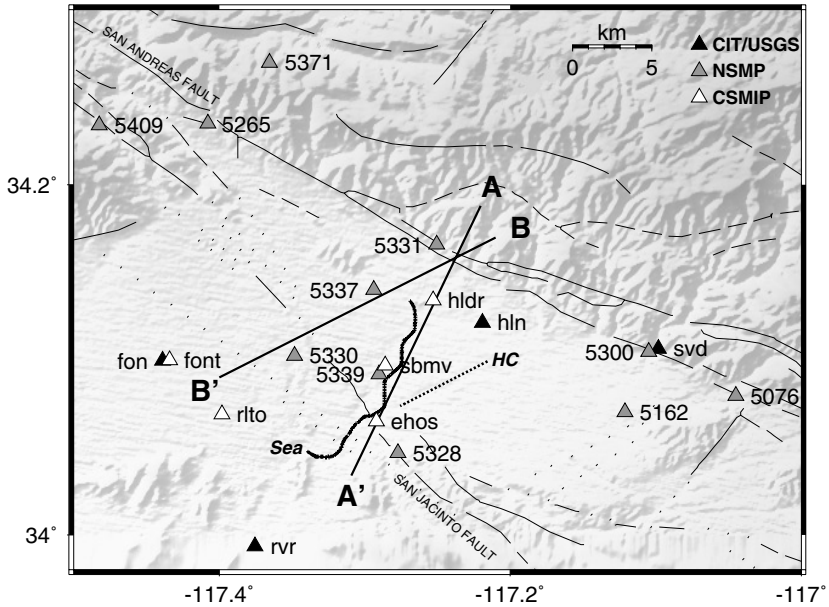


Figure 2. Detailed map view of the San Bernardino basin, which is bounded to the north by the San Andreas fault and the south by the San Jacinto fault. Faults are dotted where inferred. Sites recording strong ground motions for the Hector Mine mainshock are indicated by the triangles. The location of the refraction profile of Hadley and Combs (1974) is shown by the heavy dashed line labeled HC, and the location of the reflection survey of Stephenson *et al.* (2002) is shown by the small crosses and is labeled Sea.

the data along two profiles, labeled A and B in Figure 2. The broadband (0.04 Hz $< f <$ 25 Hz) ground velocities for these profiles are shown in Figures 3 and 4, respectively. In these figures, we show only the horizontal components (vertical motions are much smaller), and we have rotated the recorded motions to orientations of 154° and 244°, corresponding to roughly tangential and radial components relative to the earthquake.

Station 5331 is common to both profiles and is located adjacent to the San Andreas fault just north of the basin margin. The motions recorded at this site are dominated by 5- to 8-sec-period energy, which is polarized primarily on the 154° component. In addition, the waveform is relatively simple, consisting of three or four main pulses of motion. These characteristics are largely reflective of the source process. The rupture mechanism is predominantly strike slip on nearly vertical fault planes, and the azimuth to these stations is located along a maximum for *SH* radiation; thus we expect the motions to be dominant on the tangential component. Furthermore, due to the large magnitude of the event and the effects of anelastic attenuation, the energy in these broadband time histories is peaked at relatively long periods. These long-period characteristics of the Hector Mine ground motions were discussed and analyzed in detail by Boore *et al.* (2002).

The next station along profile A is hldr (located about 3 km south of 5331), and the motions here are quite similar to those observed at 5331. However, the following group of stations along this profile (sbmv, 5339, ehos, 5328) is located in the central portion of the basin, and these sites show a clear change in the amplitude and waveform character of the motions (Fig. 3). At these sites the peak amplitudes on the 154° component are roughly 50% larger than observed at 5331 and hldr, and the duration of motion is much longer and more complex. The waveforms are characterized by numerous long-period (3- to 8-sec) cycles of motion, and the largest motions are typically associated with the later arrivals. Furthermore, significant motion is also observed on the 244° component, with peak amplitudes being about 3–4 times larger than observed on the same component at the northern basin sites. Further along the profile at station rvr, the motions have decreased significantly in amplitude and do not exhibit the large late-arriving phases.

Most of the sites within the basin are classified as category CD or D (Table 1) with estimated $V_s^{30}$ in the range of 300–350 m/sec (Wills *et al.*, 2000). Thus, impedance effects may account for some of the amplification observed at the deep basin sites. However, impedance effects alone cannot explain the generation of large-amplitude later arrivals and extended durations of motions. Nor can they explain the significant scattering of energy onto the 244° component, which suggests lateral multipathing within the basin. These characteristics, coupled with the long-period nature of the response, suggest that the deeper basin structure is strongly affecting the motions as the waves propagate across this profile.

In contrast to profile A, the waveforms at sites along profile B are fairly similar for all five stations (Fig. 4). These sites show a general decrease in peak amplitude with increasing distance, and only a minor amount of scattered energy is apparent on the 244° component (most notably at stations 5337 and 5330). Again, the basin sites here are all classified as CD, similar to the deep basin sites along profile A. These characteristics suggest that the basin response varies azimuthally and is controlled by the 3D nature of the underlying structure.

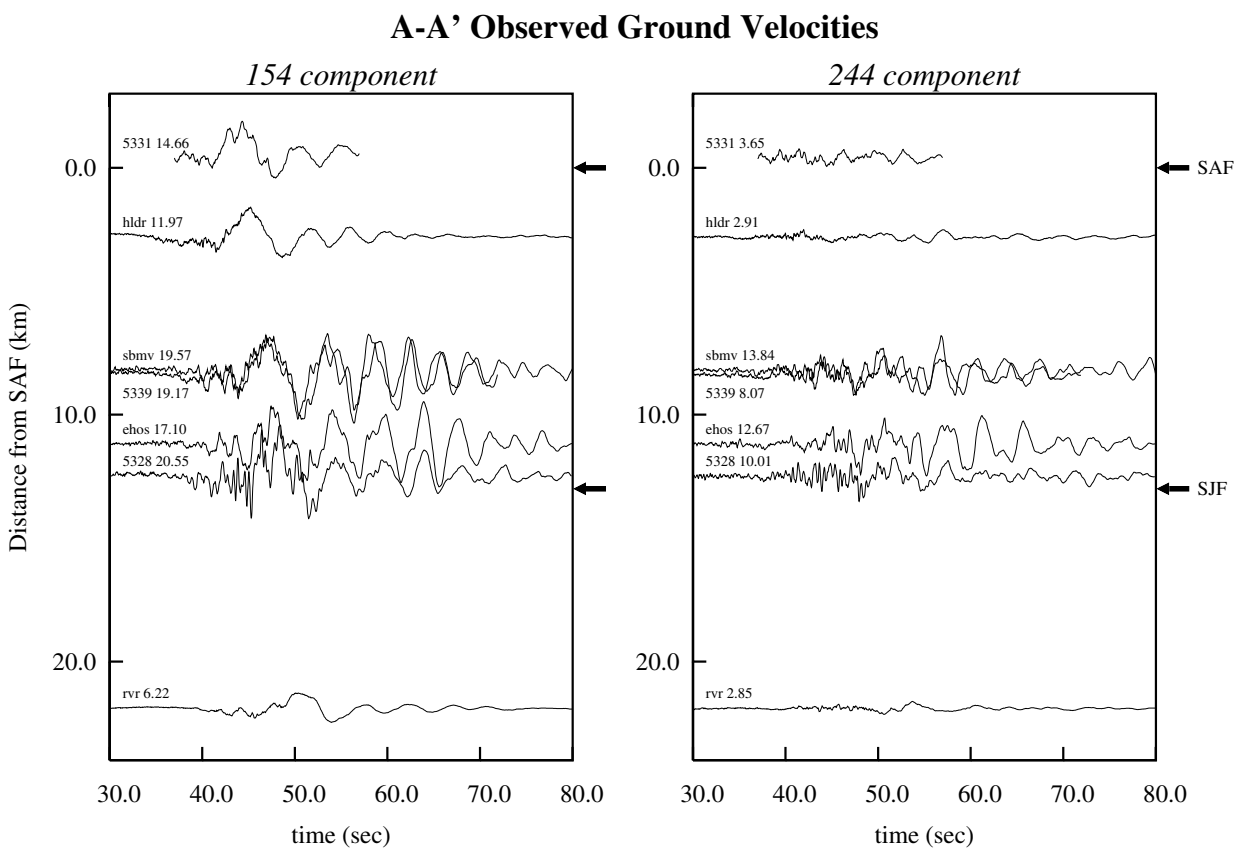


Figure 3. Horizontal-component ground velocities for stations located along profile AA′ shown in Figure 2. These ground velocities were obtained by first integrating the broadband (0.04 Hz $< f <$ 25 Hz) accelerations and then rotating into components oriented at 154° and 244° azimuths. The traces for each station are plotted relative to the distance from the San Andreas fault, with the location of the San Andreas and San Jacinto faults along the profile indicated by the arrows labeled SAF and SJF, respectively. The station name and peak amplitude is indicated above each trace. All traces are scaled to the same maximum amplitude.

## San Bernardino Basin Structure

### Geologic Setting

The San Bernardino basin is a wedge-shaped, sediment-filled structure bounded by the San Andreas fault to the north and the San Jacinto fault to the south (Fig. 2). The basin began to form about 1.5 Ma as a pull-apart structure resulting from right-lateral offset along the two bounding strike-slip faults (Morton and Matti, 1993). Sediments within the basin are primarily composed of Tertiary to Quaternary alluvial-fan deposits, and these sediments overlie pre-Tertiary igneous and metamorphic basement rocks (Dutcher and Garret, 1963). More comprehensive descriptions of the basin geology can be found in Dutcher and Garrett (1963), Morton and Matti (1993), and Stephenson *et al.* (2002).

Measurements of depth to basement rock within the basin come from a variety of sources. Several water wells (Dutcher and Garrett, 1963) and oil wells (Youngs *et al.*, 1982) penetrate to basement, particularly along the edges of the basin and also southwest of the San Jacinto fault. Wells in the central basin do not reach bedrock, but do provide a minimum constraint on its depth. Hadley and Combs (1974) conducted a seismic refraction survey in the central basin and inferred a gently southwestward-dipping basement surface at a depth of about 1 km (survey location indicated on Fig. 2).

More recently, Anderson *et al.* (2000a,b) and Langenheim *et al.* (2002) have used gravity and magnetic data to develop a 3D model of the basement topography underlying the basin. Their model is characterized by a gradual increase in sediment thickness southward from the San Andreas fault, with a maximum depth of about 1.8 km occurring just north of the San Jacinto fault. The study of Stephenson *et al.* (2002) analyzed seismic reflection data gathered along a northeast-southwest profile across the basin, as indicated in Figure 2. Although the resolution of their data begins to decrease below about 1 km, they were able to image crystalline basement along much of the profile. Their interpretation shows that the basement dips about 10° toward the southwest and reaches an inferred maximum depth of at least

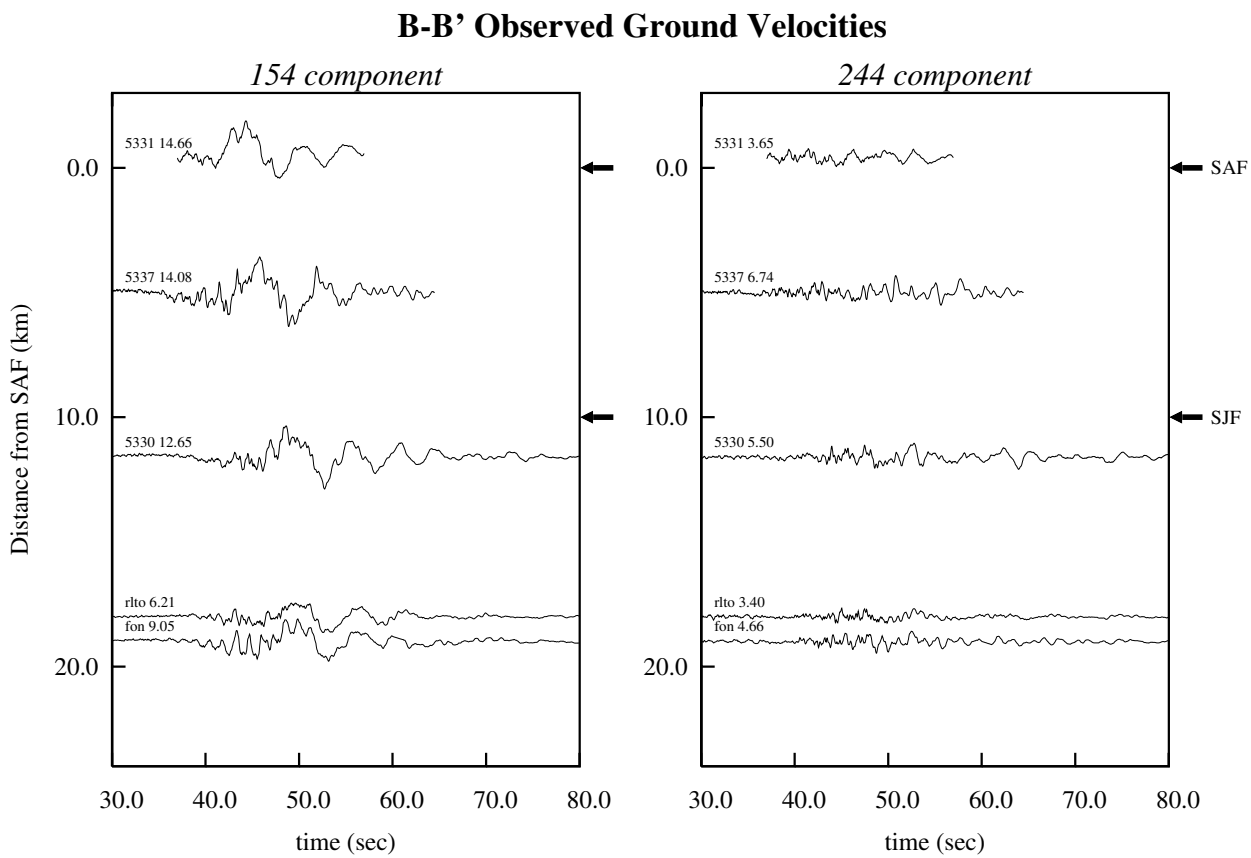


Figure 4. Same as Figure 3, except sites are located along profile BB′.

Table 1
Strong Motion Stations

| Station Code | Latitude | Longitude | $V_s^{30}$ (m/sec) | Site Type* | Operator† |
|---|---|---|---|---|---|
| hec | 34.8294 | −116.3350 | 583 | BC | CIT/USGS |
| svd | 34.1065 | −117.0983 | 583 | BC | CIT/USGS |
| hln | 34.1213 | −117.2190 | 365 | BC | CIT/USGS |
| fon | 34.0996 | −117.4388 | 365 | CD | CIT/USGS |
| rvr | 33.8822 | −117.3665 | 674 | B | CIT/USGS |
| bblk | 34.2380 | −116.9350 | 365 | CD | CSMIP |
| josh | 34.1300 | −116.3140 | 365 | CD | CSMIP |
| hldr | 34.1340 | −117.2530 | 281 | D | CSMIP |
| sbmv | 34.0970 | −117.2860 | 281 | D | CSMIP |
| ehos | 34.0650 | −117.2920 | 365 | CD | CSMIP |
| rlto | 34.0690 | −117.3980 | 365 | CD | CSMIP |
| font | 34.1000 | −117.4340 | 365 | CD | CSMIP |
| 5162 | 34.0670 | −117.1170 | 281 | D | NSMP |
| 5331 | 34.1663 | −117.2512 | 583 | BC | NSMP |
| 5076 | 34.0790 | −117.0450 | 464 | C | NSMP |
| 5337 | 34.1400 | −117.2940 | 281 | D | NSMP |
| 5330 | 34.1030 | −117.3490 | 365 | CD | NSMP |
| 5339 | 34.0910 | −117.2890 | 281 | D | NSMP |
| 5328 | 34.0470 | −117.2770 | 281 | D | NSMP |
| 5265 | 34.2350 | −117.4070 | 365 | CD | NSMP |
| 5300 | 34.1170 | −117.0980 | 365 | CD | NSMP |

*Site type and $V_s^{30}$ are from Wills *et al.* (2000). Tabulated values of $V_s^{30}$ are median estimates determined from generic profiles and site type.

†CIT = California Institute of Technology, NSMP = National Strong Motion Program, CSMIP = California Strong Motion Instrumentation Program.

1.7 km. The sediments are much thinner south of the San Jacinto fault, with approximately 1.4 km of apparent vertical displacement of the basement occurring in a narrow zone across the fault.

### Basin Velocity Models

In our analysis, we consider three models to represent the 3D basin velocity structure. Perspective views of the 3D basement surfaces for these models are shown in Figure 5, and contour plots of these surfaces are shown in map view in Figure 6. These models will be described in detail.

The first model utilizes the basement surface developed by Frankel (1993) and is hereafter referred to as "model F." The basement surface in this model is constrained primarily by the well data and refraction profile described earlier. The second model uses the basement surface of Anderson *et al.* (2000a) and is hereafter referred to as "model A." The basement surface in this model is constrained primarily by gravity data and is also consistent with the seismic reflection model of Stephenson *et al.* (2002). The third model is from

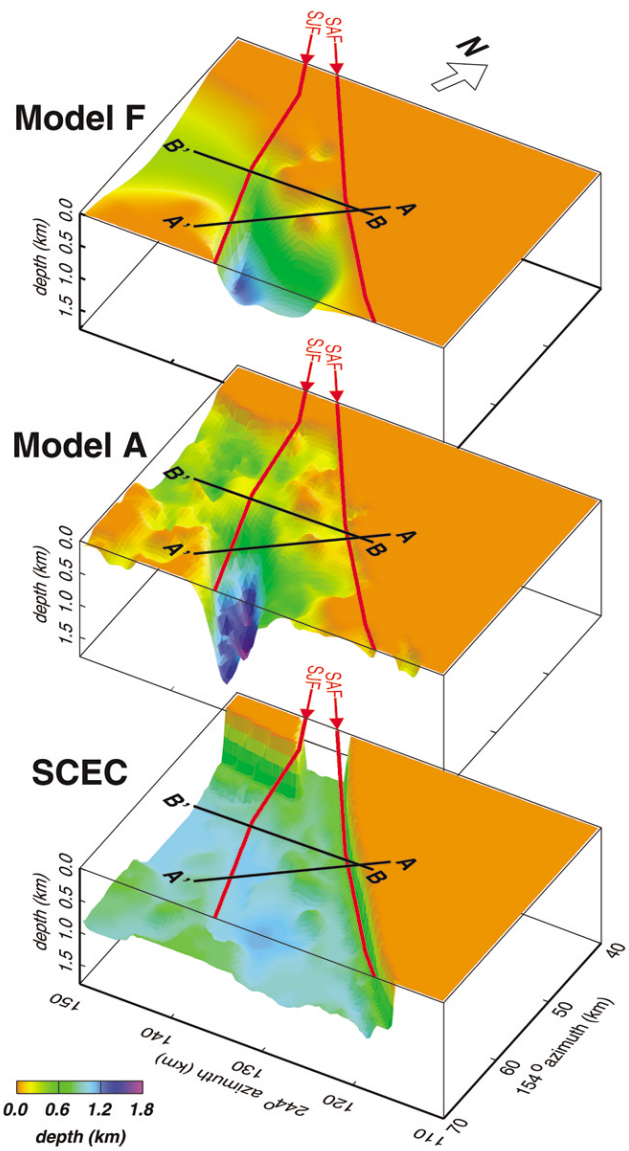


Figure 5. Perspective view of the basement surface for each of the three basin models considered in the simulations. The view is toward the northwest, roughly along the strike of the San Andreas and San Jacinto faults (indicated by the red lines). The surface locations of profiles AA′ and BB′ are also shown.

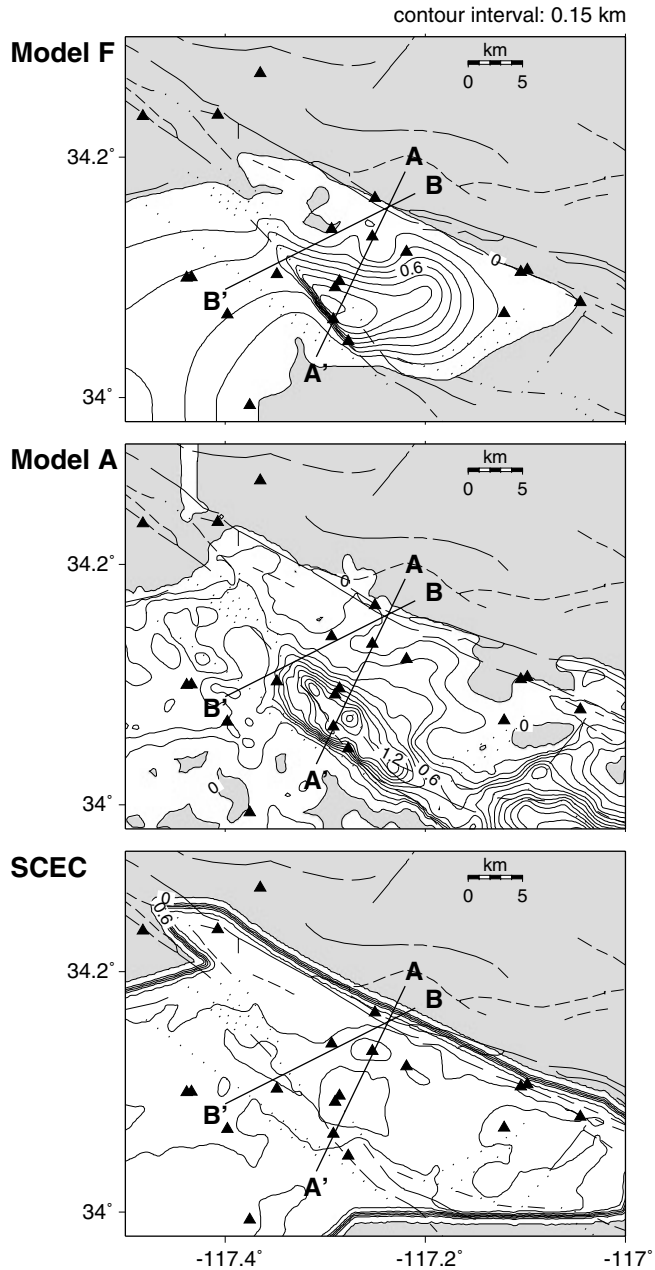


Figure 6. Contour plots of the basement surface for each of the three basin models. Contour interval is 0.15 km. The triangles indicate locations of the strong motion sites shown in Figure 2. Gray shading is bedrock.

the SCEC version 3 seismic velocity model (Kohler *et al.*, 2003) and is hereafter referred to as the "SCEC model." The depth to basement in the SCEC model is essentially constant at about 1 km depth, constrained primarily by the base of water-bearing strata (Department of Water Resources, 1970) and the Hadley and Combs (1974) refraction profile.

In a broad sense, the basement structures of models F and A are fairly similar. Both are characterized by a gradual increase in sediment thickness southwestward from the San Andreas fault, with an abrupt shallowing in basement depth along the San Jacinto fault zone. The maximum depth in model F is about 1.4 km, and for model A it is about 1.8 km. In both models, the deepest part of the basin is found just north of the San Jacinto fault. At shorter wavelengths, model A exhibits much more complexity than model F, resulting from the dense coverage of gravity stations in this region. Additionally, model A contains some structural control outside of the immediate basin region (e.g., to the southeast) that is not included in model F.

The basement structure of the SCEC model is noticeably different than the other two models. This model is characterized by a sharp step in the basement surface along the San Andreas fault and a nearly uniform depth of about 1 km covering the entire basin. Furthermore, there is little structural relief in the basement topography along the San Jacinto fault.

A key attribute of the models is the specification of the velocity structure within the basin sediments. The original model of Frankel (1993) has a constant $V_s$ within the basin of 600 m/sec, and the structural model of Anderson *et al.* (2000a) has no velocity control. For these models, we impose a stratified velocity structure within the sediments based on the *P* velocity estimates given by Hadley and Combs (1974). We assume a $V_p/V_s$ ratio that decreases from 3 at the surface to about 2 for the deepest sediments, along with corresponding density values. Unfortunately, no direct information is known about the *S* velocities in the deep basin, and our estimates of $V_p/V_s$ ratios and densities are guided mainly by our previous basin-modeling experience (e.g., Graves *et al.*, 1998). Velocities within the SCEC model are derived using a rule-based formulation that relates sediment age and depth of burial to *P*-wave velocity. For the San Bernardino basin, this formulation is calibrated to match the velocities given in the Hadley and Combs (1974) refraction model. Empirical relations are then used to determine density and $V_s$ from the $V_p$ values. Magistrale *et al.* (2000) gave a detailed explanation of the rule-based formulation and its implementation. Due to computational limitations, the minimum $V_s$ was fixed at 600 m/sec in all of the models.

Figure 7 compares shear velocity cross sections taken from the three models along profiles A and B. These cross sections illustrate the general similarities between models F and A, as well as the noticeable differences between these models and the SCEC model. Along profile A, models F and A exhibit a gently sloping basement interface beginning at the San Andreas fault and reaching a maximum depth just before the San Jacinto fault zone. The SCEC model has a sharp, vertical basin edge located slightly northeast of the San Andreas fault, with a nearly uniform basin thickness of 1 km. Along profile B, the structure of the SCEC model is essentially the same as in profile A. However, models F and A indicate a significant thinning of the basin sediments along this profile. In spite of their similarities along these profiles, we also note that the structure of models F and A do contain some subtle differences (e.g., depth to basement, shape of the basement interface, location of the San Jacinto fault) that can lead to significant differences in ground-motion response, as will be discussed later.

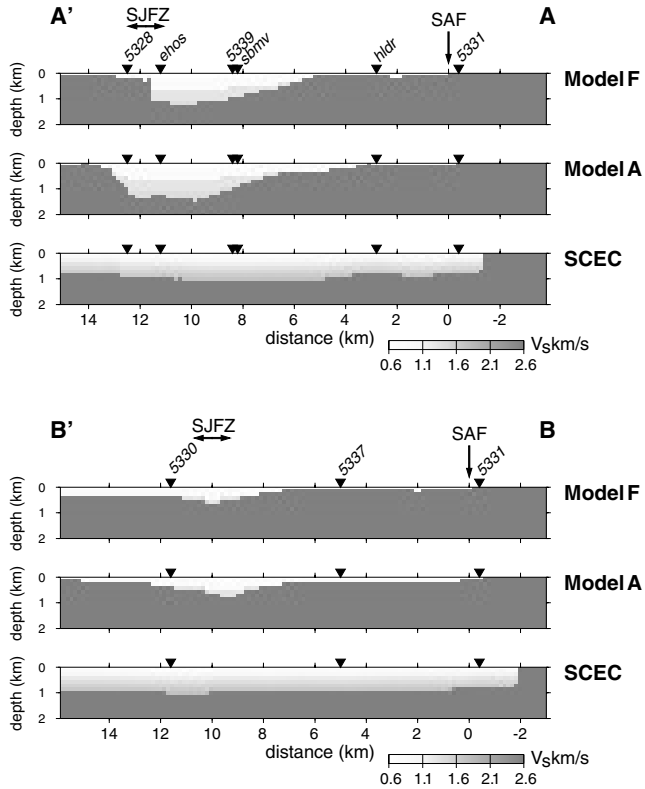


Figure 7. Cross sections of shear-wave velocity along profiles AA′ and BB′ for the three basin models. The projected locations of the strong motion stations are indicated for each profile, along with the locations of the San Andreas fault (SAF) and the San Jacinto fault zone (SJFZ).

Figure 8 compares 1D velocity and density profiles taken from the models at two sites in the northern basin region (5331 and hldr) and two deep basin sites (sbmv and ehos). Site 5331 is located just north of the San Andreas fault and is classified as category BC, while the basin sites hldr, sbmv, and ehos are classified as category CD (Table 1) (Wills *et al.*, 2000). At 5331 and hldr, the SCEC model has much lower velocities in the upper 800 m than the other models. This is reflective of the difference between the flat basin bottom in the SCEC model and the gradually sloping basement interface in models F and A. The profiles at sites sbmv and ehos are much more similar for the three models.

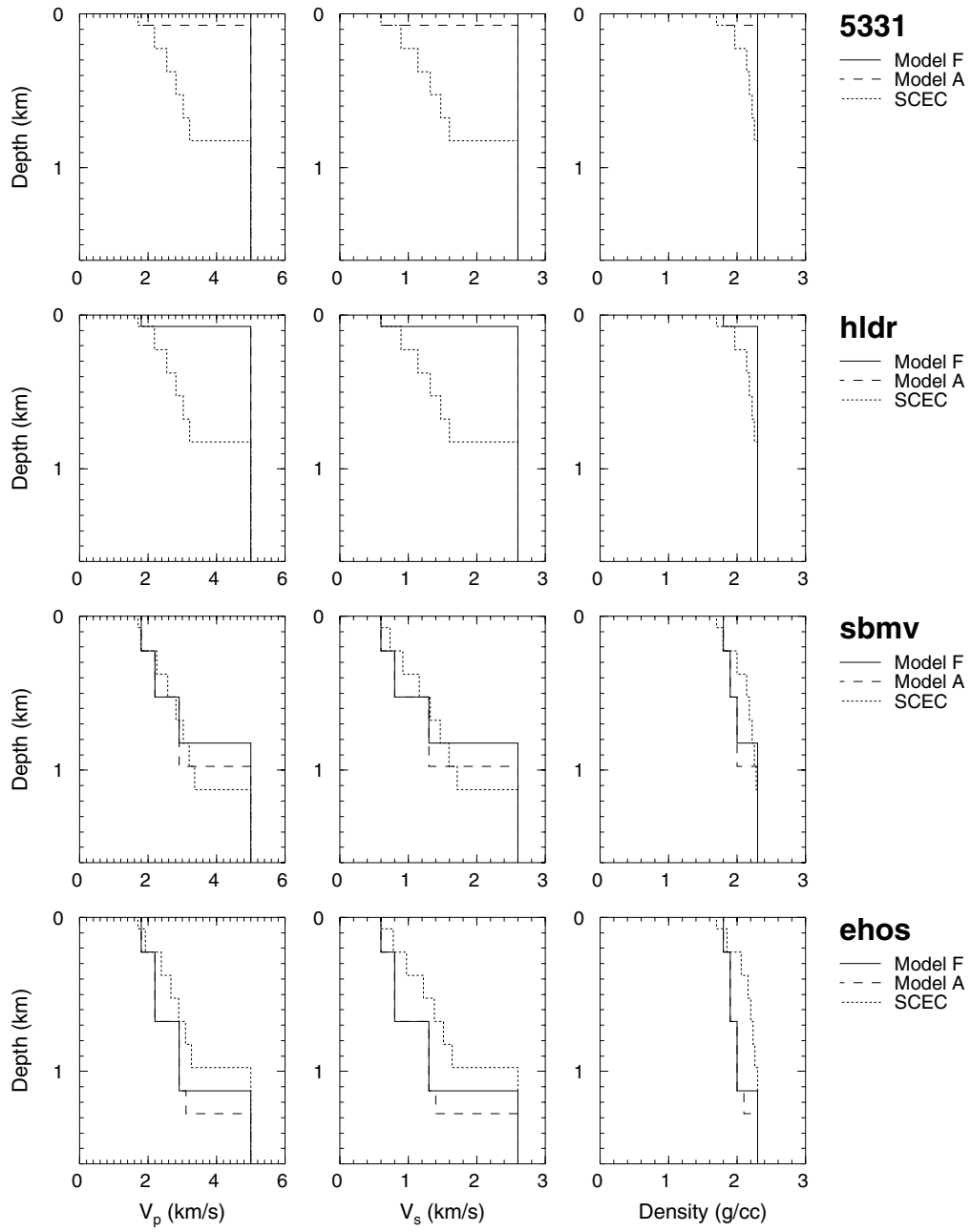


Figure 8. Vertical profiles of velocity and density from the three basin models taken at four strong motion recording sites near San Bernardino. See Figure 2 for site locations.

The main differences here are slight variations in the basement depth of the three models and somewhat lower $V_s$ and density gradients in the SCEC model compared to the others.

For all three models, the media outside of the basin is represented by the Mojave model of Jones and Helmberger (1998). This was done to ensure consistency with our chosen source rupture model for the Hector Mine event and to also concentrate our analysis on the variability of the ground-motion response arising solely from differences in the proposed basin structures. The structure of the Mojave model is listed in Table 2. In order to incorporate this structure within the SCEC model, we simply replace the regional tomographic crustal structure in the original SCEC model with the Mojave structure.

## Ground-Motion Simulations

We use the model of Ji *et al.* (2002) to represent the source rupture process of the Hector Mine mainshock. This source model consists of a kinematic description of the spatial and temporal evolution of the slip process along the three fault segments shown in Figure 1. The fault displacement is

Table 2
Mojave Crustal Model

| $V_p$ (km/sec) | $V_s$ (km/sec) | Density (g/cm$^3$) | Depth (km) |
|---|---|---|---|
| 5.0 | 2.6 | 2.4 | 2.5 |
| 5.5 | 3.45 | 2.4 | 5.5 |
| 6.3 | 3.6 | 2.67 | 28.0 |
| 7.85 | 4.4 | 3.42 | – |

almost pure right-lateral strike slip, and the fault planes are all nearly vertical. In this model, the largest slip values (about 7 m) are located on two asperities adjacent to the hypocenter. The slip rise time on these asperities is relatively long at about 6 sec, and this long rise time tends to accentuate the longer-period energy in the ground motions, as discussed earlier.

Ground motions are simulated using the staggered-grid finite-difference (FD) method of Graves (1996). Our FD model covers an area of 116 km by 162 km (Fig. 1) and extends to a depth of 50 km. To reduce the total number of model nodes, we use the variable grid spacing technique of Pitarka (1998). Within the shallow basin, the horizontal and vertical grid steps are 200 and 150 m, respectively. At a sampling of 5 grid points per shear wavelength in the lowest velocity regions (600 m/sec), this parameterization gives a frequency resolution of 0.6 Hz, or about 1.7 sec. In the higher velocity regions outside the basin and at depth, the grid spacing increases in a manner that maintains the frequency resolution criterion. Anelastic attenuation was modeled using the method of Graves (1996), with $Q_s$ values specified using the relation $Q_s = 100 \cdot V_s$ (where $V_s$ is in kilometers per second) and setting the reference frequency at 0.3 Hz.

As a first step in the modeling procedure, we compare observed and simulated motions at several sites outside the basin region (Fig. 9). For this calculation, the FD model consists of only the background Mojave velocity structure. This allows us to confirm the adequacy of the source representation in our FD model and also to assess how well we are modeling the propagation of energy into the basin region. The waveforms displayed in Figure 9 are ground velocities that have been low-pass filtered using a two-pass fourth-order Butterworth operator with a corner at 0.5 Hz.

Three of the sites (hec, josh, and svd) were directly used in the source inversion of Ji *et al.* (2002), and as we expect, the simulated motions match the recorded waveforms quite well at these sites. At the other sites (bblk, 5076, and 5331), the simulation also provides a reasonably good match to the observations, particularly at the longer periods. Stations 5076, svd, and 5331 all lie along the northern edge of the basin (Fig. 2). At all of these sites the main long-period (about 8-sec) pulse of motion is modeled quite well. For 5076 and 5331, the simulated arrivals following the main pulse have a noticeably stronger shorter-period content (about 3–4 sec) than the recorded motions, and the simulation tends to underpredict the total duration of the observed waveform. We attribute this mismatch in the shorter-period response to source and regional wave propagation complexities that are not fully constrained at these sites since they were not explicitly included in the source inversion. Nonetheless, the overall comparison of the recorded and simulated waveforms at these sites is reasonably favorable, indicating that our simulation model adequately captures the main long-period characteristics of the motions as they enter the basin region.

Figures 10, 11, and 12 compare observed ground velocities with those simulated for each of the three basin models. All of the ground motions shown in these figures have been low-pass filtered using a two-pass fourth-order Butterworth operator with a corner at 0.5 Hz. The sites shown in Figure 10 are located along the northern basin margin, those shown in Figure 11 are from the central basin, and those shown in Figure 12 are from the southwestern portion of the basin region (see Fig. 2). Each of these figures will be discussed in more detail.

At sites along the northern basin margin (Fig. 10), the observed motions are characterized by a large long-period pulse of motion on the 154° component, which is followed by several cycles of smaller-amplitude motion. Motions on the 244° component are typically a factor of 2 or more smaller in amplitude than those on the 154° component. In general, these features are reproduced fairly well at all sites by models A and F. In addition, at svd, the SCEC model also produces motions similar to the data and those of the other models. However, at the other stations, following the main long-period pulse of motion, the motions from the SCEC model are dominated by large-amplitude, shorter-period arrivals, which are not apparent in the observed motions. This is especially evident at stations 5337 and 5265.

For the sites shown in Figure 10, the basin sediments are quite thin in models A and F; thus there is little basin response in the simulated ground motions. In contrast, the SCEC model has about 1 km of low-velocity sediments underlying each of these sites with the sharp basin edge boundary located just to the northeast (see Figs. 6 and 7). This type of basin margin is very efficient at trapping and amplifying motions, particularly at periods around 1 or 2 sec (e.g., Kawase, 1996). The large amplification seen in the SCEC model occurs at about 2-sec period and is most pronounced when the incoming wave field has a relatively strong component of shorter-period energy and for stations located more than 1–2 km from the basin edge (e.g., hldr, 5337, and 5265).

The sites shown in Figure 11 are located in the central basin region, and the observed ground motions at these sites exhibit significant basin response effects. These include amplified levels of motion, extended durations of shaking, and a strong response on the 244° component. To varying degrees of success, each of the simulations qualitatively matches the characteristics seen in the observed motions. These basin response effects are created by surface waves that are generated along the northern basin margin as the

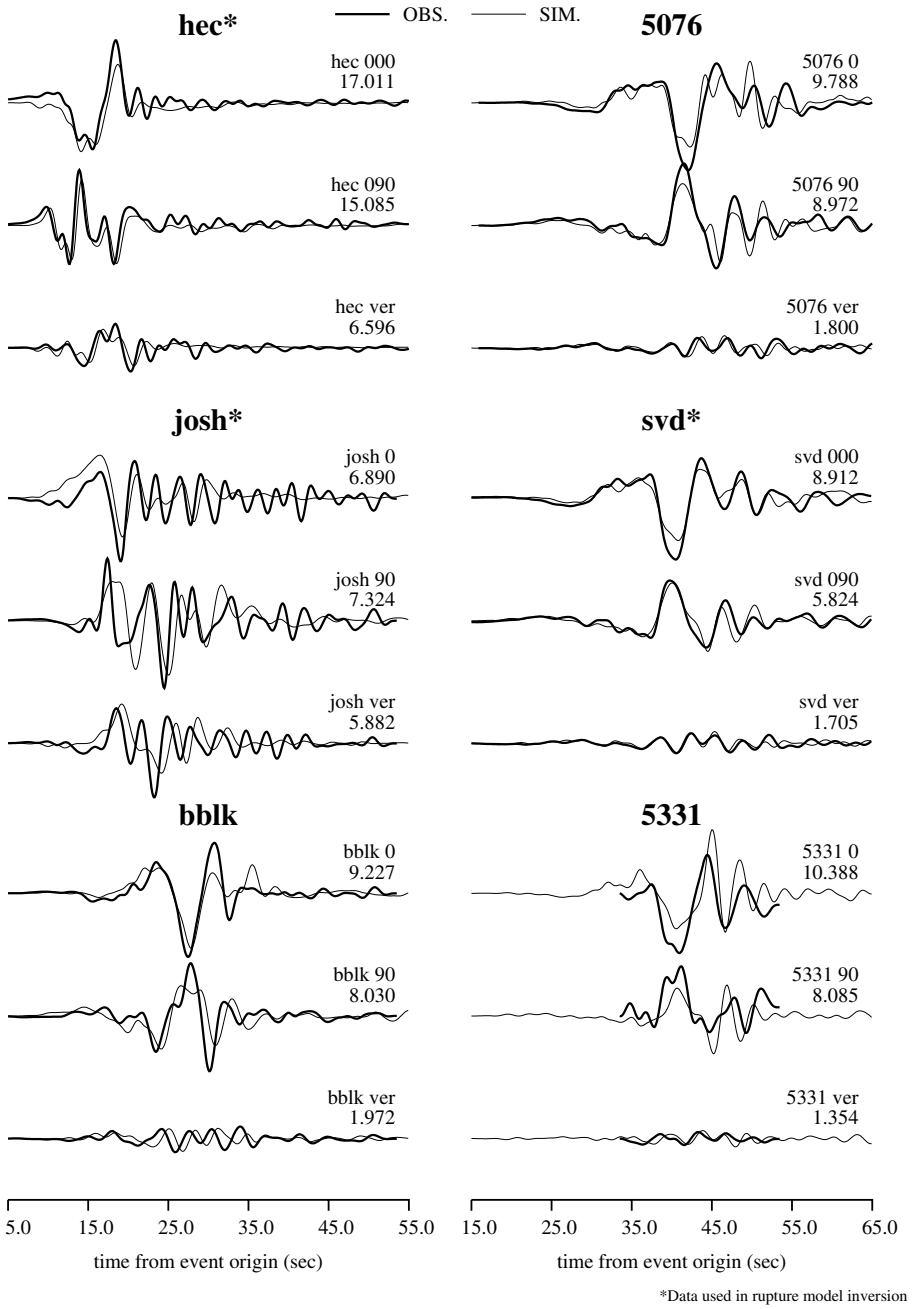


Figure 9. Comparison of recorded (thick traces) three-component ground velocities with those simulated (thin traces) at six sites using the 1D Mojave crustal model. All traces have been low-pass filtered using a two-pass fourth-order Butterworth operator with a corner at 0.5 Hz. For each station, the order of the traces are north–south (top), east–west (middle) and up–down (bottom). The peak amplitude of the recorded motion for each component is shown at the upper right of the trace, and all of the traces for each station are scaled to the same maximum amplitude.

incoming wave field interacts and becomes trapped within the low-velocity sediments. The sharp basin edge in the SCEC model traps energy very quickly at the basin margin, producing large-amplitude surface waves immediately adjacent to this boundary, which then decay rapidly with increasing distance. The more gently sloping basin interface in models A and F traps energy more slowly, but over a greater lateral extent. Thus, the surface waves in these models tend to grow in amplitude with increasing distance from the basin margin, until the basin reaches its maximum depth.

Of the three models, the SCEC model provides a somewhat better match to the amplitudes and waveforms at sites

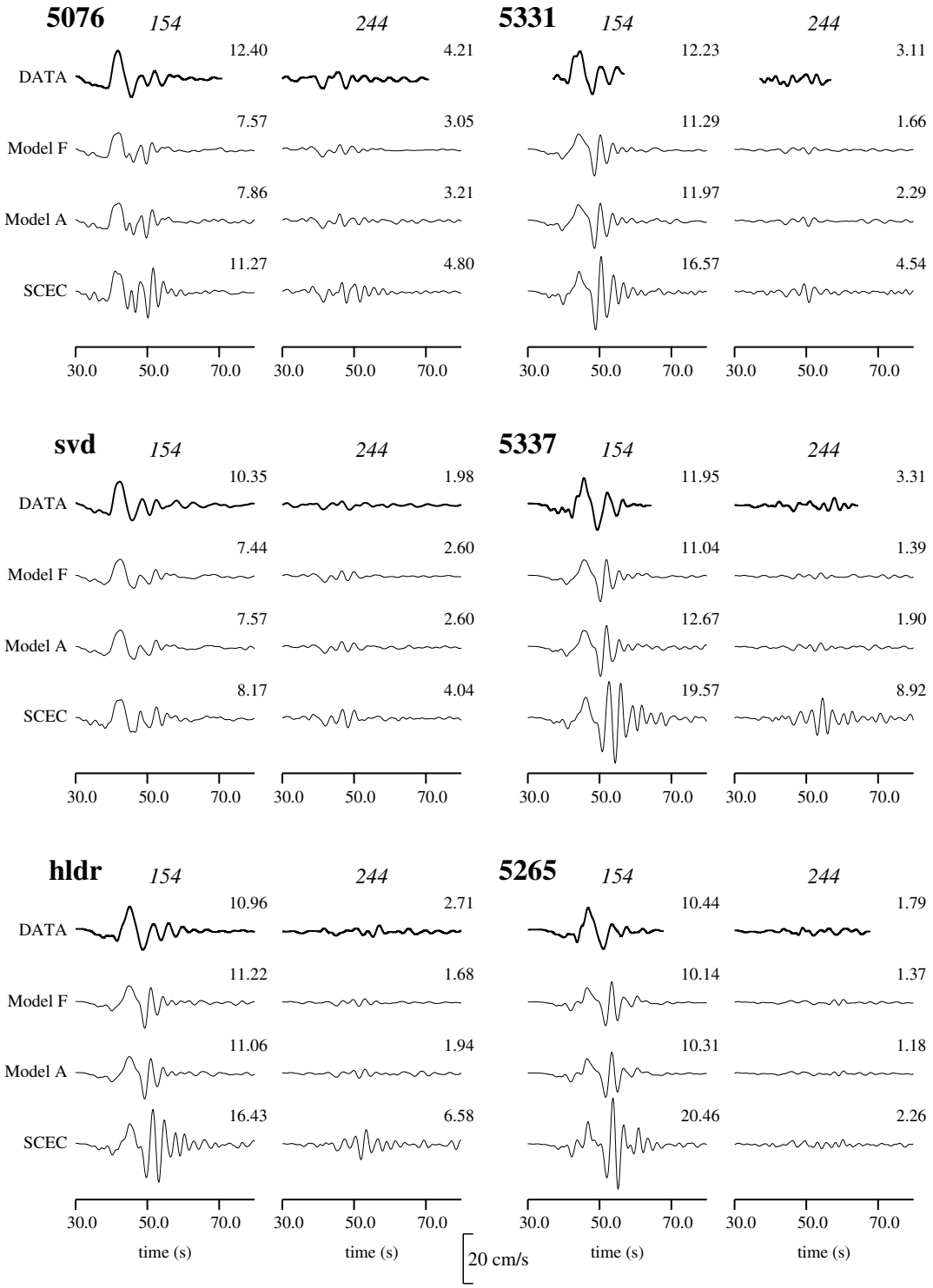


Figure 10. Detailed comparison of recorded horizontal ground velocities with those simulated for the three basin velocity structures at stations located along the northern basin margin. All traces have been low-pass filtered using a two-pass fourth-order Butterworth operator with a corner at 0.5 Hz. For each station, the top trace is the observed motion and the simulated responses are plotted below. The peak amplitude is shown at the top right of each trace. All of the traces are scaled to the same maximum amplitude, with the scale bar shown at the bottom center of the figure. Station locations are indicated in Figure 2.

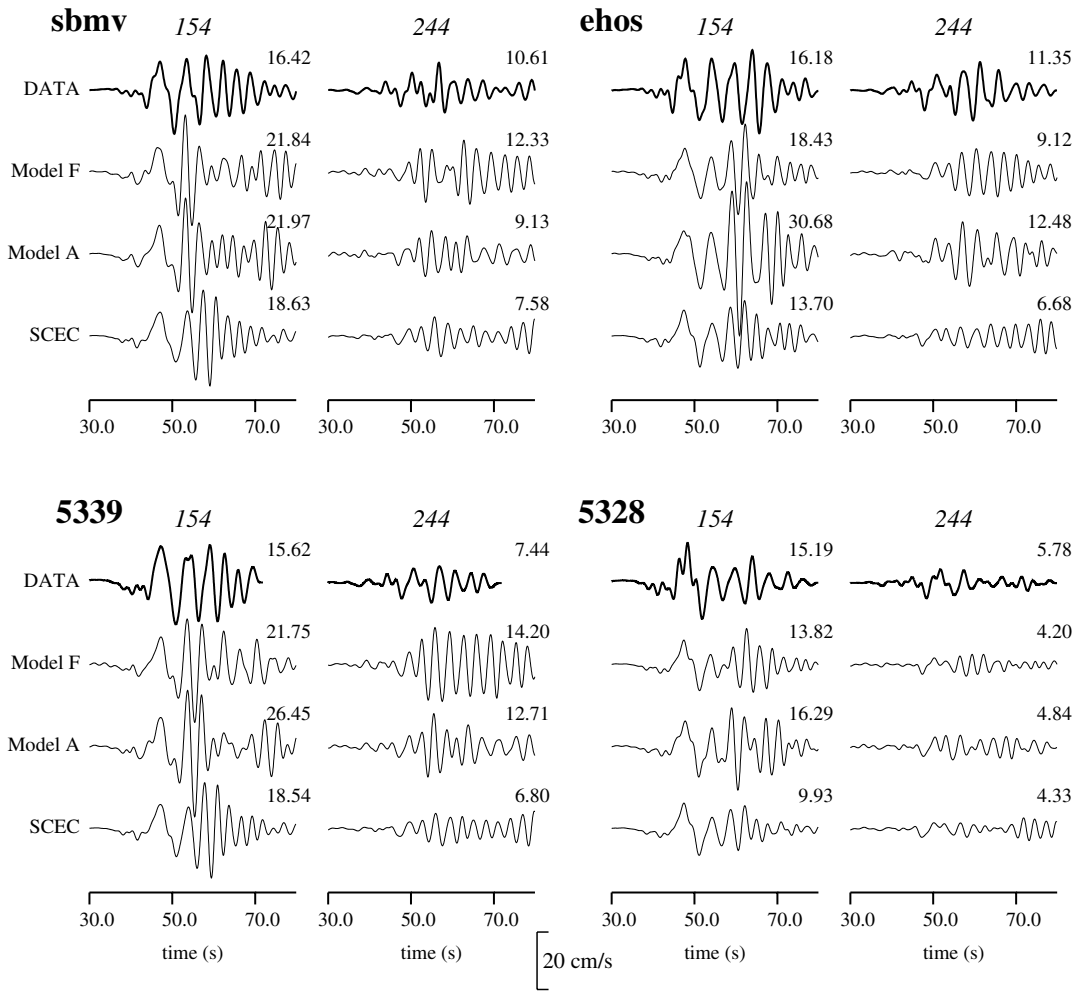


Figure 11. Same as Figure 10, except for stations located in the central basin.

sbmv and 5339, whereas model F provides a better match to the motions at sites ehos and 5328. At all sites, the waveforms simulated with model A are fairly similar to those of model F, although the amplitudes are generally higher on the 154° component. This suggests that the shear velocities assigned to the deep basin sediments in model A may be too low or that the basin structure in this model may be too deep.

In Figure 12, three of the stations are basin sites located west of the San Jacinto fault (5330, rlto, and fon) and the fourth is a rock site located south of the basin region (rvr). As discussed previously (see Fig. 4), the motions at these sites are relatively simple, being more similar to the motions observed north of the basin region than those at sites in the central basin. Both models A and F do reasonably well at reproducing the waveforms at these sites. The SCEC model predicts large-amplitude basin surface waves at these sites, which are not observed in the data. Due to the uplifted basement along the San Jacinto fault in models A and F, the surface waves generated in these models are confined to the central basin region to the north and east of this fault structure. The SCEC model, lacking the uplifted basement structure, allows the surface waves to continue propagating to sites south and west of the San Jacinto fault.

Figure 13 provides a map view comparison of observed peak ground velocity with those simulated for each of the three basin models. The two horizontal components are displayed separately, and both the data and simulations have been low-pass filtered using a two-pass fourth-order Butterworth operator with a corner at 0.5 Hz. As discussed earlier, the largest amplitudes in the recorded motions are for sites located in the central basin. This is true for both horizontal components. Both models A and F exhibit a spatial distribution quite similar to the data, with the amplitudes increasing toward the central basin and smaller amplitudes in the north and southwest basin regions. Model F provides the best overall match to the pattern and magnitude of the observed amplitudes, while model A overpredicts the amplitudes in the central basin on the 154° component. The largest amplitudes in the SCEC model are in the northern basin region, and this model overpredicts the observed amplitudes in both the northern and western portions of the basin.

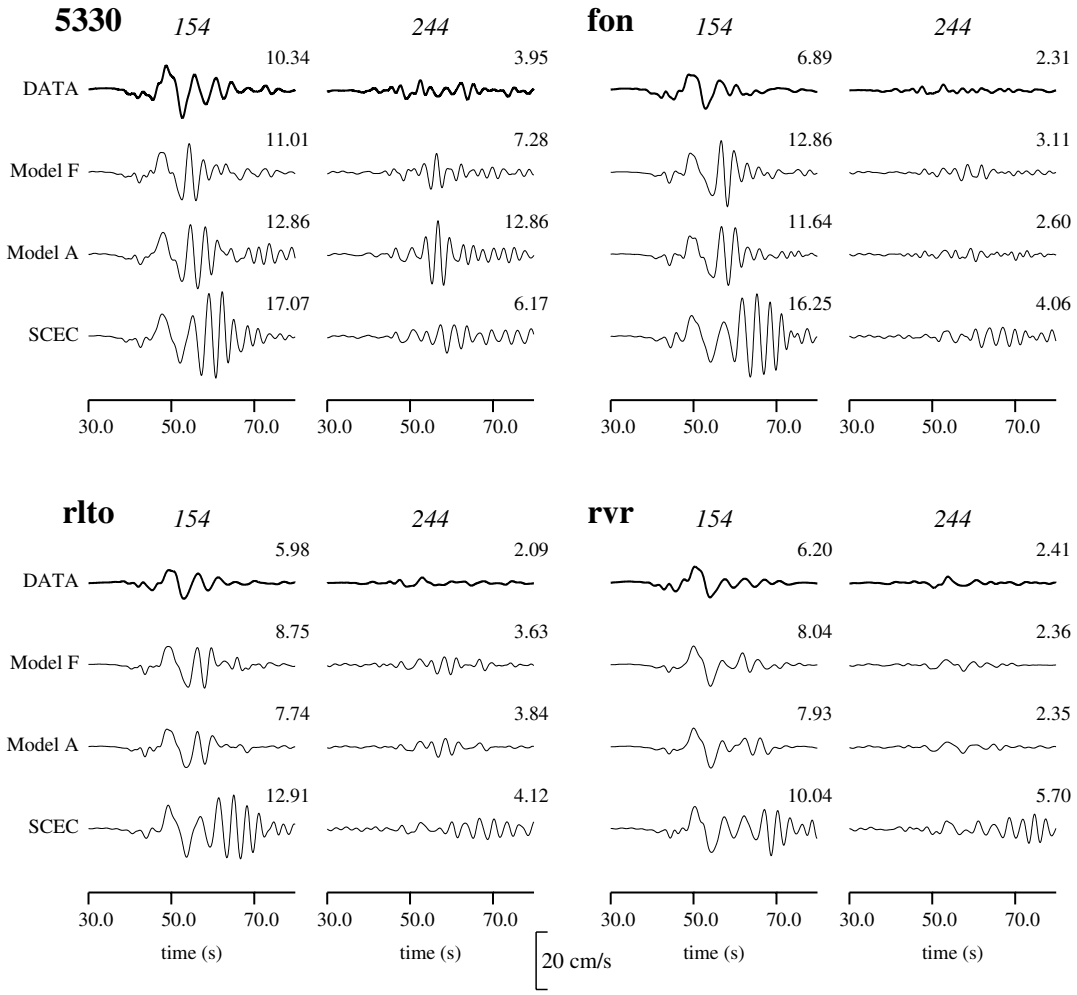


Figure 12. Same as Figure 10, except for stations located in the southwestern portion of the basin.

## Discussion

The simulation results presented in the previous section suggest that a sloping basement structure, such as in models A and F, works well at reproducing the the main long-period characteristics of the observed ground motions for the Hector Mine earthquake. This type of structure is consistent with recent geological and geophysical investigations in the San Bernardino region that indicate that the basin sediments are shallow in the northern basin and gradually increase in thickness toward the southwest. In contrast, a structure with a sharp basin margin, such as in the SCEC version 3 model, produces a zone of large amplification adjacent to the basin edge (i.e., the basin edge effect; Kawase, 1996) that is not seen in the ground-motion data. As of the writing of this manuscript, the SCEC model is being refined to include a sloping basement surface from the Anderson *et al.* (2000a) gravity model (Magistrale, 2002). Structurally, the new SCEC model (version 4) should be similar to model A used in this study; however, the sediment velocities may be significantly different due to the rule-based formulation employed in the SCEC model. Further evaluation of the ground-motion response of this new model will be necessary once it becomes available.

Our results also highlight the importance of accurate characterization of source complexity and wave propagation effects outside of the basin in order to adequately represent the incoming wave field. This can be difficult for large events such as Hector Mine because of the inherent trade-offs between these two effects. For example, the motions at station svd are modeled quite well in our simulations, which is not surprising since this site was directly used in the derivation of the source model (Ji *et al.*, 2002). At other nearby sites along the basin margin, the simulations are not quite as good, particularly at the shorter-periods where our simulations tend to overpredict the observed amplitudes (e.g., bblk, 5076, and 5331 in Fig. 9).

In the source inversion process, ground-motion waveforms are constructed by determining the optimal time lag and weighting for the various phases that produce the best fit to the observed motions at each site. However, there are

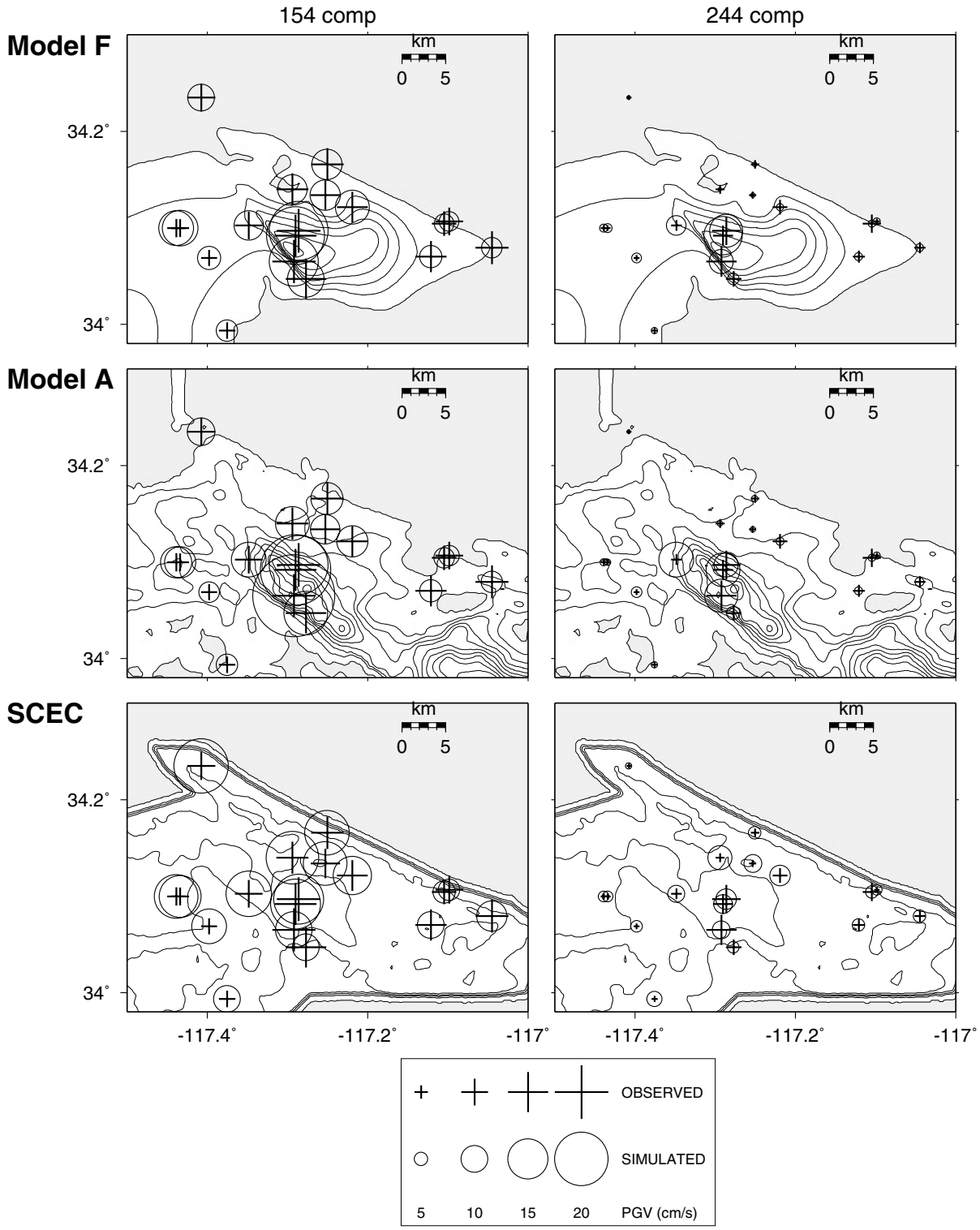


Figure 13. Comparison of observed and simulated peak velocity for the three basin velocity models as measured at each of the strong motion stations. The peak values are determined from the filtered ($T > 2$ sec) time histories. Observed values are shown with crosses and simulated values are shown with circles, with the size of the symbols scaling with the measured peak amplitude. The symbols are plotted at the corresponding station location and superimposed on the basement contours (Fig. 6) for each velocity model. The left panels show the 154° component, and the right panels show the 244° component.

no guarantees that this will produce an optimal waveform fit for sites not used in the inversion. We suspect that this is the case at stations bblk, 5076, and 5331. The effect is particularly noticeable at the shorter-periods where slight changes in the timing of individual phases can produce significant changes in the simulated waveforms. The overprediction of the shorter-period energy at the basin sites in our simulations may result, in part, from this effect in the incoming wave field. One possible way to circumvent this problem is to use ground-motion data from smaller nearby events, which presumably have simpler source characteristics. An analysis following this approach has recently been applied to the San Bernardino region using data from the 2001 $M_w$ 4.6 Big Bear Lake earthquake with reasonable success down to periods of about 2–3 sec (Graves, 2002).

Numerically, the modeling results in this study are valid for periods greater than 2 sec. One of our future goals is to push the modeling threshold down to periods approaching 1 sec. To accomplish this will require more knowledge and a better representation not only of the source process as discussed earlier, but also of the sediment velocities and basin structure on a much smaller scale than exists in the current models. For example, most of the sites within the basin are classified as CD or D with $V_s^{30}$ in the range of 300–350 m/sec (Wills *et al.*, 2000; Gibbs *et al.*, 2001), which is significantly lower than the minimum $V_s$ of 600 m/sec used in the current study. In fact, the recent modeling work for the Big Bear Lake earthquake of Graves (2002) finds an improved fit at periods of 2–3 sec for many of the basin waveforms when this minimum $V_s$ value is reduced to 400 m/sec.

However, reducing the minimum velocity threshold is only one aspect of the problem that needs to be addressed. Since the shorter-period motions become increasingly sensitive to structural variability on rather short length scales (about 50–100 m for 1-sec period), much more detailed information on the fine-scale structure of the shallow basin geology needs to be developed as well. Recent near-surface shear velocity logging studies may help in this effort (e.g., Gibbs *et al.*, 2001).

Additionally, constraints on the exact nature of the deep basin structure are still somewhat limited. The seismic reflection (Stephenson *et al.*, 2002) and refraction (Hadley and Combs, 1974) data do not directly image structures below about 1 km depth. Furthermore, these studies are conducted along linear arrays and sample only a small extent of the basin. The gravity analysis (Anderson *et al.*, 2000a) is attractive because it provides a detailed representation of the basement interface throughout the basin region. However, it is dependent on the assumed density contrasts, which are not well controlled for the deeper sediments. Recent work combining analyses of gravity and magnetic field data shows promise in reducing the uncertainty of the deeper basement structure (Langenheim *et al.*, 2002).

The significance of the deep basin structure on the long-period ground-motion response is exemplified in the simulations at ehos using models A and F (Fig. 11). The primary difference between these models is the structure and depth of the deep basin. Model A extends to a maximum depth of about 1.8 km, while model F has a maximum depth of about 1.4 km. Clearly, this difference can have an significant impact on the ground-motion response, with the peak simulated motions at ehos being about 1.7 times larger for model A than model F. For both models, the largest amplitude arrivals at this site are late-arriving surface waves with a period of about 3–4 sec. Understanding the nature of the response for the deep basin has important implications for estimating the ground-shaking hazard for future events in this region. This is particularly true for large nearby ruptures on the San Andreas or San Jacinto faults, which will generate a much stronger response at periods around 1–2 sec than is seen in the data for the more distant Hector Mine earthquake. The preliminary analysis of Graves (2001) has shown that the response of the basin is different for San Andreas ruptures than for San Jacinto ruptures due to the asymmetric basin geometry. Developing better constraints on the deep basin structure should help to reduce the uncertainty in these types of ground-motion estimates.

## Conclusions

The long-period ground motions observed in the San Bernardino region during the 1999 Hector Mine earthquake exhibit strong basin response effects, including amplification of motions, generation of basin surface waves, and extended durations of shaking. We can model the main characteristics of these motions reasonably well for periods of 4–5 sec and longer using a basin structure developed from recent geological and geophysical studies. Our modeling suggests that the basin structure has a sloping basement interface along its northern margin and extends to a maximum depth of about 1.4–1.8 km just north of the San Jacinto fault. The basement surface then shallows abruptly along this fault structure to an average depth of about 300 m. Our study also demonstrates the utility of integrating geological, geophysical, and seismological observations in the development and validation of 3D velocity models. Finally, this study represents a first step toward developing a comprehensive 3D velocity structure for this region that can then be used to simulate strong ground motions for future scenario earthquakes.

## Acknowledgments

The authors are grateful for the in-depth and constructive review comments provided by David Boore, Harold Magistrale, Bill Stephenson, and Art Frankel. Several of the figures for the manuscript were prepared using GMT software (Wessel and Smith, 1991). This work was sponsored in part by USGS external program grants 1434-HQ-98-GR-00027 and 02-HQ-GR-0096 and funding from the Southern California Earthquake Center (SCEC). SCEC is funded by NSF Cooperative Agreement EAR-8920136 and USGS Cooperative Agreements 14-08-0001-A0899 and 1434-HQ-97AG01718. The SCEC Contribution Number for this article is 712.

## References

Anderson, M. L., R. C. Jachens, and J. C. Matti (2000a). Structural model of the San Bernardino strike-slip basin southern California, from regional gravity and aeromagnetic data, *2000 Geol. Soc. Am. Ann. Mtg. Abstract*, Reno, Nevada, 13–16 November 2000.

Anderson, M. L., C. W. Roberts, and R. C. Jachens (2000b). Principal facts for gravity stations in the vicinity of San Bernardino, southern California, *U.S. Geol. Surv. Open-File Rept. 00-193*, 32 pp.

Boore, D. M., C. D. Stephens, and W. B. Joyner (2002). Comments on baseline correction of digital strong motion data: examples from the 1999 Hector Mine, California, earthquake, *Bull. Seism. Soc. Am.* **92,** 1543–1560.

Department of Water Resources (1970). Meeting water demands in the Chino–Riverside area, Bulletin 104-3, Appendix A, The Resources Agency, Sacramento, California, 108 pp.

Dutcher, L. C., and A. A. Garrett (1963). Geologic and hydrologic features of the San Bernardino area, California, U.S. Geol. Surv. water supply paper 1419, 114 pp.

Frankel, A. (1993). Three-dimensional simulations of ground motions in the San Bernardino Valley, California, for hypothetical earthquakes on the San Andreas fault, *Bull. Seism. Soc. Am.* **83,** 1020–1041.

Frankel, A. (1994). Dense array recordings in the San Bernardino Valley of Landers–Big Bear aftershocks: basin surface waves, Moho reflections, and three-dimensional simulations, *Bull. Seism. Soc. Am.* **84,** 613–624.

Gibbs, J. F., D. M. Boore, J. C. Tinsley, and C. S. Mueller (2001). Borehole *P*- and *S*-wave velocity at thirteen stations in southern California, *U.S. Geol. Surv. Open-File Rept. 01-506*, 121 pp.

Graves, R. W. (1996). Simulating seismic wave propagation in 3D elastic media using staggered grid finite differences, *Bull. Seism. Soc. Am.* **86,** 1091–1106.

Graves, R. W. (2001). Long period ground motions in the San Bernardino region for hypothetical San Andreas and San Jancinto earthquakes, *EOS* **82,** no. 47 (Fall Meet. Suppl.), Abstract S32D-09.

Graves, R. W. (2002). The seismic response of the San Bernardino basin region, *EOS* **83,** no. 47 (Fall Meet. Suppl.), Abstract S21A-0968.

Graves, R. W., A. Pitarka, and P. G. Somerville (1998). Ground motion amplification in the Santa Monica area: effects of shallow basin edge structure, *Bull. Seism. Soc. Am.* **88,** 1224–1242.

Hadley, D., and J. Combs (1974). Microearthquake distribution and mechanisms of faulting in the Fontana–San Bernardino area of southern California, *Bull. Seism. Soc. Am.* **64,** 1477–1500.

Hauksson, E., L. M. Jones, and K. Hutton. (2002). The 1999 $M_w$ 7.1 Hector Mine, California, earthquake sequence: complex conjugate strike-slip faulting, *Bull. Seism. Soc. Am.* **92,** 1154–1170.

Ji, C., D. J. Wald, and D. V. Helmberger (2002). Source description of the 1999 Hector Mine, California earthquake, part II: complexity of slip history, *Bull. Seism. Soc. Am.* **92,** 1208–1226.

Jones, L. E., and D. V. Helmberger (1998). Earthquake source parameters and fault kinematics in the eastern California shear zone, *Bull. Seism. Soc. Am.* **88,** 1337–1352.

Kawase, H. (1996). The cause of the damage belt in Kobe: "The basin-edge effect," constructive interference of the direct *S*-wave with the basin-induced diffracted/Rayleigh waves, *Seism. Res. Lett.* **67,** 25–34.

Kohler, M., H. Magistrale, and R. Clayton (2003). Mantle heterogeneities and the SCEC Reference Three-Dimensional Seismic Velocity Model version 3, *Bull. Seism. Soc. Am.* **93,** 757–774.

Langenheim, V. E., M. Anderson, R. C. Jachens, J. C. Matti, D. M. Morton, and T. King (2002). 3D model of subsurface structure between the San Andreas and San Jacinto faults, southern California, based on gravity and magnetic data, *2002 SCEC Ann. Mtg. Abstracts*, Oxnard, California, 7–11 September.

Magistrale, H. (2002). Improvements to the SCEC community velocity model, *2002 SCEC Ann. Mtg. Abstracts*, Oxnard, California, 7–11 September.

Magistrale, H., S. Day, R. Clayton, and R. Graves (2000). The SCEC southern California reference three dimensional seismic velocity model version 2, *Bull. Seism. Soc. Am.* **90,** S65–S76.

Morton, D. M., and J. C. Matti (1993). Extension and contraction within an evolving divergent strike-slip fault complex: the San Andreas and San Jacinto fault zones at their convergence in southern California, Geol. Soc. Am. Memoir, Vol. 178, 217–230.

Pitarka, A. (1998). 3D elastic finite difference modeling of seismic wave propagation using staggered grid with non-uniform spacing, *Bull. Seism. Soc. Am.* **88,** 54–68.

Stephenson, W. J., J. K. Odum, R. A. Williams, and M. L. Anderson (2002). Delineation of faulting and basin geometry along a seismic reflection transect in urbanized San Bernardino valley, California, *Bull. Seism. Soc. Am.* **92,** 2504–2520.

Wessel, P., and W. H. F. Smith (1991). Free software helps map and display data, *EOS* **72,** no. 441, 445–446.

Wills, C. J., M. Peterson, W. A. Bryant, M. Reichle, G. J. Saucedo, S. Tan, G. Taylor, and J. Treiman (2000). A site conditions map for California based on geology and shear wave velocity, *Bull. Seism. Soc. Am.* **90,** S187–S208.

Working Group on California Earthquake Probabilities (WGCEP) (1995). Seismic Hazards in southern California: probable earthquakes, 1994 to 2024, *Bull. Seism. Soc. Am.* **85,** 379–439.

Youngs, L. G., S. F. Bezore, R. H. Chapman, and G. W. Chase (1982). Resource investigations of low and moderate temperature geothermal areas in San Bernardino, California, CDMG Open-File Report 82-11, 242 pp.

URS Group, Inc.
566 El Dorado Street
Pasadena, California 91101
robert_graves@urscorp.com
(R.W.G.)

U.S. Geological Survey
1711 Illinois Street
Golden, Colorado 80401
wald@usgs.gov
(D.J.W.)

Manuscript received 31 January 2003.